

The Electronics and Data Acquisition System of the DarkSide Dark Matter Search

The DarkSide Collaboration; P. Agnes¹, T. Alexander², A. Alton³, K. Arisaka⁴, H. O. Back⁵, B. Baldin⁶, K. Biery⁶, G. Bonfini⁷, M. Bossa⁸, A. Brigatti⁹, J. Brodsky⁵, F. Budano¹⁰, L. Cadonati², F. Calaprice⁵, N. Canci⁴, A. Candela⁷, H. Cao⁵, M. Cariello¹¹, P. Cavalcante⁷, A. Chavarria¹², A. Chepurnov¹³, A. G. Cocco¹⁴, L. Crippa⁹, D. D'Angelo⁹, M. D'Incecco⁷, S. Davini¹⁵, M. De Deo⁷, A. Derbin¹⁶, A. Devoto¹⁷, F. Di Eusano⁵, G. Di Pietro⁹, E. Edkins¹⁸, A. Empl¹⁵, A. Fan⁴, G. Fiorillo¹⁴, K. Fomenko¹⁹, G. Forster², D. Franco¹, F. Gabriele⁷, C. Galbiati⁵, A. Goretti⁵, L. Grandi¹², M. Gromov¹³, M. Y. Guan²⁰, Y. Guardincerri⁶, B. Hackett¹⁸, K. Herner⁶, E. Hungerford¹⁵, Al. Ianni⁷, An. Ianni⁵, C. Jollet²¹, K. Keeter²², C. Kendziora⁶, S. Kidner²³, V. Kobychiev²⁴, G. Koh⁵, D. Korablev¹⁹, G. Korga¹⁵, A. Kurlej², P. X. Li²⁰, B. Loer⁵, P. Lombardi⁹, C. Love²⁵, L. Ludhova⁹, S. Luitz²⁶, Y. Q. Ma²⁰, I. Machulin^{27,28}, A. Mandarano¹⁰, S. M. Mari¹⁰, J. Maricic¹⁸, L. Marini¹⁰, J. Martoff²⁵, A. Mereaglia²¹, E. Meroni⁹, P. D. Meyers⁵, R. Milincic¹⁸, D. Montanari⁶, M. Montuschi⁷, M. E. Monzani²⁶, P. Mosteiro⁵, B. Mount²², V. Muratova¹⁶, P. Musico¹¹, A. Nelson⁵, S. Odrowski⁷, M. Okounkoa⁵, M. Orsini⁷, F. Ortica¹⁹, L. Pagani¹¹, M. Pallavicini¹¹, E. Pantic^{4,32}, L. Papp²³, S. Parmeggiano⁹, Bob Parsells⁵, K. Pelczar³¹, N. Pelliccia²⁹, S. Perasso¹, A. Pocar², S. Pordes⁶, D. Pugachev²⁷, H. Qian⁵, K. Randle², G. Ranucci⁹, A. Razeto⁷, B. Reinhold¹⁸, A. Renshaw⁴, A. Romani²⁹, B. Rossi⁵, N. Rossi⁷, S. D. Rountree²³, D. Sablone¹⁵, P. Saggese⁷, R. Saldanha¹², W. Sands⁵, S. Sangiorgio³⁰, E. Segreto⁷, D. Semenov¹⁶, E. Shields⁵, M. Skorokhvatov^{27,28}, O. Smirnov¹⁹, A. Sotnikov¹⁹, C. Stanford⁵, Suvorov⁴, R. Tartaglia¹⁷, J. Tatarowicz²⁵, G. Testera¹¹, A. Tonazzo¹, E. Unzhakov¹⁶, R. B. Vogelaar²³, M. Wada⁵, S. E. Walker¹⁴, H. Wang⁴, Y. Wang²⁸, A. Watson²⁵, S. Westerdale⁵, M. Wojcik³¹, A. Wright⁵, X. Xiang⁵, J. Xu⁵, C. G. Yang²⁰, J. Yoo⁶, S. Zavatarelli¹¹, A. Zec², C. Zhu⁵, G. Zuzel³¹

(1) APC, Université ParisDiderot, Sorbonne Paris Cité, 75205 Paris, France;

(2) Physics Department, University of Massachusetts, Amherst, MA 01003, USA;

(3) Physics and Astronomy Department, Augustana College, Sioux Falls, SD 57197, USA;

(4) Physics and Astronomy Department, University of California, Los Angeles, CA 90095, USA;

(5) Physics Department, Princeton University, Princeton, NJ 08544, USA;

(6) Fermi National Accelerator Laboratory, Batavia, IL 60510, USA;

(7) Laboratori Nazionali del Gran Sasso, 67010 Assergi, Italy;

- (8) Gran Sasso Science Institute, 67100 L'Aquila, Italy;
- (9) Physics Department, Università degli Studi and INFN, 20133 Milano, Italy;
- (10) Physics Department, Università degli Studi Roma Tre and INFN, 00146 Roma, Italy;
- (11) Physics Department, Università degli Studi and INFN, Genova, 16146, Italy;
- (12) Kavli Institute, Enrico Fermi Institute, and Department of Physics, University of Chicago, Chicago, IL 60637, USA;
- (13) Skobeltsyn Institute of Nuclear Physics, Lomonosov Moscow State University, Moscow 119991 ;
- (14) Physics Department, Università degli Studi Federico II and INFN, 80126, Napoli, Italy;
- (15) Department of Physics, University of Houston, Houston, TX 77204, USA
- (16) Petersburg Nuclear Physics Institute, Gatchina 188350, Russia;
- (17) Physics Department, Università degli Studi and INFN, Cagliari 09042, Italy;
- (18) Department of Physics and Astronomy, University of Hawai'i, Honolulu, HI 96822, HI;
- (19) Joint Institute for Nuclear Research, Dubna 141980, Russia;
- (20) Institute for High Energy Physics, Beijing 100049, China;
- (21) IPHC, (19) Université de Strasbourg, CNRS/IN2P3, 67037 Strasbourg, France;
- (22) School of Natural Sciences, Black Hills State University, Spearfish, SD 57799, USA;
- (23) Physics Department, Virginia Tech, Blacksburg, VA 24061, USA;
- (24) Institute for Nuclear Research, National Academy of Sciences of Ukraine, Kiev 03680, Ukraine;
- (25) Physics Department, Temple University, Philadelphia, PA 19122, USA;
- (26) SLAC National Accelerator Laboratory, Menlo Park, CA 94025, USA;
- (27) National Research Center Kurchatov Institute, Moscow 123182, Russia;
- (28) National Research Nuclear University MEPhI (Moscow Engineering Physics Institute), 115409 Moscow, Russia;
- (29) Department of Chemistry, Biology and Biotechnology, Università degli Studi and INFN, 06123 Perugia, Italy;
- (30) Lawrence Livermore National Laboratory, 7000 East Avenue, Livermore, CA 94550, USA;
- (31) Smoluchowski Institute of Physics, Jagiellonian University, 30059 Krakow, Poland;
- (32) Physics Department, University of California, Davis, CA 95616, USA;

Abstract. It is generally inferred from astronomical measurements that Dark Matter (DM) comprises approximately 27% of the energy-density of the universe. If DM is a subatomic particle, a possible candidate is a Weakly Interacting Massive Particle (WIMP), and the DarkSide-50 (DS) experiment is a direct search for evidence of WIMP-nuclear collisions. DS is located underground at the Laboratori Nazionali del Gran Sasso (LNGS) in Italy, and consists of three active, embedded components; an outer water veto (CTF), a liquid scintillator veto (LSV), and a liquid argon (LAr) time projection chamber (TPC). This paper describes the data acquisition and electronic systems of the DS detectors, designed to detect the residual ionization from such collisions.

1. The DarkSide Experiment

A wide range of astronomical evidence suggests the existence of a gravitationally-interacting, non-luminous component of the universe which has yet to be identified. This Dark Matter (DM) component comprises approximately 27% of the energy density of the universe, and is responsible for the galactic structures visible today [1]. There are viable arguments that DM could be composed of Weakly Interacting Massive Particles (WIMP), and the DarkSide-50 (DS) experiment is a search for the ionization produced by WIMP-nuclear collisions as a fixed detector on Earth moves through the WIMP field of the Milky Way. Such interactions are rare, and impart recoil energies to a nucleus of at most a few tens of keV [2]. Thus to reach the required sensitivities, detectors having large target masses and background suppression are needed. A number of technologies are now used for direct detection of dark matter WIMPs. These include; cryogenic bolometers with ionization or scintillation detection (CDMS [3], EDELWEISS [4], CRESST [5]); sodium/cesium iodide scintillation detectors (DAMA/LIBRA [6], KIMS [7]); bubble chambers (PICASSO [8], COUPP [9]); a point contact germanium detector (CoGeNT [10]); and liquid noble gas detectors (Xenon: XENON [11], [12], LUX [13], XMASS [14] and Argon: mini-CLEAN/DEAP [15], ArDM [16], DarkSide-50 [17]).

The heart of the DarkSide-50 (DS) experiment is a 50 kg Time Projection Chamber (TPC) which is a two-phase liquid argon (LAr) detector designed to achieve background-free operation for at least 0.1 tonne-year of exposure. This TPC exploits the extraordinary pulse shape discrimination (PSD) of LAr [18] providing powerful rejection of electromagnetic (electron or gamma induced) signals. Cosmogenic background is suppressed to very low levels by mounting DS at a 3800 mwe (water equivalent) depth at the Laboratori Nazionali del Gran Sasso (LNGS) laboratory [19] [20], and surrounding the TPC with two nested veto shields of high purity water (CTF) and liquid scintillator (LSV), Figure 1. In addition, local radioactive background is significantly reduced by efficient chemical and cryogenic purification methods [21], and the use of underground argon (UAr) obtained from gas wells depleted in the radioactive ^{39}Ar isotope [22]. Despite the small detector size, DS has a sensitivity to WIMP-nucleon cross sections of approximately 10^{-45} cm^2 for a WIMP mass of 100 GeV/ c^2 .

This paper describes the DS electronics, the data collection and event-building systems (DAQ), and the slow control and data monitoring systems of the experiment.

2. Detector Systems

DarkSide-50 consists of three embedded detector systems. Viewed from the inner to the outer these system are: a LAr TPC, a liquid scintillator system (LSV) composed of 50% PPO + 50% TMB [23], and a water Cherenkov Veto system (CTF) which also acts to shield the LSV and TPC from local radioactive background. An enclosed clean room (CLR) sits atop the CTF, and is used to insert and provide access to the TPC when the water and scintillator are removed. The CLR isolates the TPC and its components from surface radioactivity, particular radon, during assembly.

Electrical connections to the TPC, approximately 5-10 /m in length, are made through vacuum-tight pipes from the TPC to a feed-through in a flange on the floor

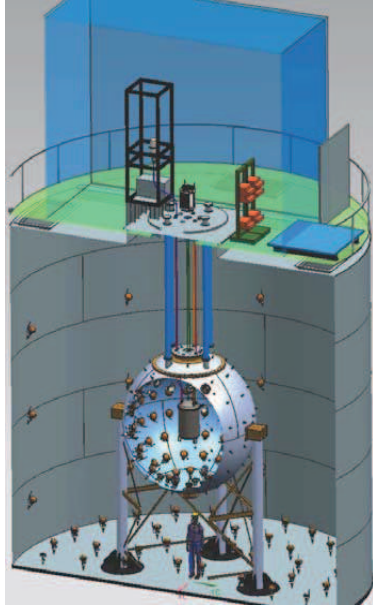


Figure 1. The DarkSide experimental layout showing the water and scintillation vetoes, the TPC cryostat, and the clean room (CLR) atop the CTF

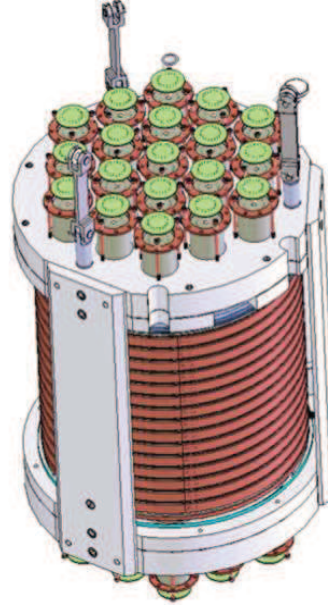


Figure 2. The DarkSide TPC showing the PMT and field shaping rings. The TPC is immersed in LAr but has a gas pocket just below the upper PMT window.

of the CLR. To minimize noise on the PMT signals, the TPC front end electronics are located in the CLR racks just above the flange, which is as close as possible to the TPC. Readouts of the veto signals from the LSV and CTF, however, are patched through the side of the CTF to a control room (CoR) by cables some 40 m in length. Thus synchronization of these systems is one of the electronic challenges addressed below.

3. The TPC

The TPC, shown in Figure 2, is a cylindrical detector containing 50 kg of LAr. The inner cylindrical surface of the detector is a Teflon reflector coated with wavelength shifter (tetraphenyl butadiene (TPB)). The coating absorbs the 128 nm scintillation photons emitted by the LAr ionization, and re-emits visible photons which are viewed by thirty-eight Hamamatsu low-background R11065 PMT [27]. The PMT are divided equally between the top and bottom surfaces of the TPC, and receive the wavelength-shifted light through fused silica windows. These windows are also coated with the wavelength shifter on the inner surfaces and have transparent conductive layers of indium tin oxide (ITO) evaporated on both the inner and outer surfaces. Coating both surfaces with ITO allows

the inner window surface to serve as a grounded anode (top) and a high voltage cathode (bottom) of the TPC, while maintaining the outer surfaces at the average PMT photocathode potential. The fused silica anode (top) window has a cylindrical rim extending downward into the TPC to form a 1 cm-thick gas pocket above the LAr. High voltage is applied between the TPC cathode and anode to produce, by field shaping rings, a uniform electric field throughout the active volume. Light due to ionization in the LAr (S1) is collected by the PMT. Electrons from this ionization drift upwards in the electric field, eventually reaching the liquid surface where they are extracted, and accelerated in the gas pocket producing secondary ionization light (S2). The drift time of the ionization charge, and the amplitude of the light signal in the gas are adjustable by varying the potentials on the cathode and an extraction grid which is placed just below the LAr surface. This design not only provides three-dimensional information of the position of the event in the LAr, but also allows discrimination between the ionization due to Ar recoils and that of electromagnetic interactions, (*ie* β or γ events). This technique mainly uses the ratio of the fast component of the (S1) ionization signal (the first 90 ns) to its total integral [18]. Thus, it is important to minimize electronic noise and use a low frequency cutoff to accurately determine the total pulse shape.

3.1. TPC Front-End Electronics

As explained above, wavelength-shifted light from an event in the LAr is viewed through fused silica windows by 38 low-background PMT. Although the PMT are not placed in the sensitive volume of the TPC, they are immersed in LAr and operate at a temperature of approximately 87 K. After extensive testing, it was found that charge accumulation on internal components in the PMT induced erratic behavior. This is mitigated by decreasing the tube voltage, reducing the PMT gain to a few $\times 10^5$. However, the reduced gain requires a local pre-amplifier operating at LAr temperatures to drive the signals through the approximate 5-10 m of cable to the amplifiers in the CLR without significant contribution from noise and dispersion. Both the TPC amplifiers and digitizers are located in racks in the CLR, just above the CTF.

3.1.1. Pre-amplifier The cryogenic pre-amplifier is constructed using discrete components as illustrated in the sketch in Figure 4. Power-loss density is important as the pre-amplifier is mounted on the PMT base which is immersed in LAr. Local boiling can cause a multitude of problems with high voltages, electronics, and TPC operations. Consequently the pre-amplifier is designed with a total power consumption less than 90 mW/channel. It is also constructed to be as radio-pure as possible, requiring the use of a Cirlex [28] circuit board, low radioactive components, and avoidance of copper-beryllium (CuBe) connectors. Its input impedance is determined by the internal, stray capacitance of the PMT and signal shaping to optimize the signal-to-noise ratio. The relatively high-load resistance produces a passive gain with respect to a PMT coupling which is back terminated by 50 Ω . The active gain of the pre-amplifier is 3 V/V, for a total 24V/V compared to the output without a pre-amplifier. The maximum output is 3V providing a dynamic range in excess of 1500 photoelectrons (pe). Pole-zero cancellation is applied to the output signals sent to the amplifier. High quality, double shielded cables [29] are used to transmit these signals from the TPC to the amplifiers in the CLR.

3.1.2. Noise Abatement Special care was taken to maintain high signal integrity during the experimental implementation. Thus, “screw-on” RF connectors (SMA) and double shielded signal cables are used wherever possible. The cryogenic pre-amplifiers used surface mounted components with a grounded, full copper backplane, and the power supply was carefully filtered to reduce noise components. Impedance matching and signal reflection of the output signals were also adjusted to minimize cross-talk and electromagnetic interference (EMI).

While the hermetically sealed cryostat containing the pre-amplifiers should provide shielding from external noise sources, penetrations by signal, test, and power cables conveyed external noise to the pre-amplifiers. This is exacerbated by the requirement that the PMT anodes were maintained at ground potential in order to use DC signal coupling. This requires that the metal envelope of the PMT remained floating at the cathode potential and could not be easily shielded. Thus interference pick-up by the PMT dynodes becomes impressed on the photocurrents prior to amplification. Given the above issues, noise abatement required simultaneously considering the full detector system, including cryogenics and the slow control components, as well as the TPC electronics. It was found that cryogenic pump-drivers, system switching power supplies, telecommunication transceivers, and high voltage supplies all provided contribution to the signal noise. These were addressed in situ after installation.

Pump motor controllers are especially noisy sources, because most send unfiltered and un-shielded signals to the appliance which they control. These sources of noise were mitigated by variac-based sinusoidal motor controls. Noisy switching power supplies were identified and individually treated by filtering or replacing supplies with linear components. In particular noise from the PMT high voltage (HV) supplies was reduced by adding filters on the HV output.

Ground loops were also mitigated by floating all connections through the cryostat wall. At the same time, all cable shields were connected via low-inductance AC coupling to the cryostat surface, to reduce the RF energy which would otherwise enter the cryostat. As a result, the noise at the output of the amplifier chain is dominated by the pre-amplifier electronic noise floor. Thus there are no noise-dominant spectral components within the frequency range of interest. The output noise is $70\ \mu\text{V}$ for an active bandwidth of 150 MHz.

3.1.3. Amplifier The amplifier in the CLR provides further amplification and signal conditioning. The coupling between the pre-amplifier and the amplifier boards is illustrated in Figure 5. One amplifier module handles five channels and provides the following outputs for each channel.

- An amplified output with gain of 10 V/V and an input noise equivalent of $20\ \mu\text{V}$ over a bandwidth of 200 MHz. This output is typically used for monitoring the performance of specific channels
- A shaped output with a gain of 10 V/V with a bandwidth of 90 MHz and a noise equivalent of $15\ \mu\text{V}$. The bandwidth is matched to the sampling frequency of the CAEN V1720 digitizer which samples at 250 MS/s



Figure 3. A picture of the cryogenic pre-amplifier mounted of the PMT base

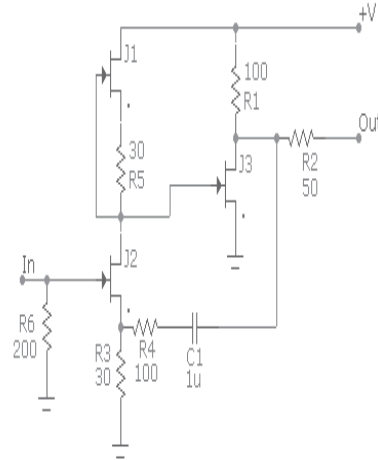


Figure 4. The circuit diagram of the cryogenic pre-amplifier

- An attenuated output with gain of 0.5 V/V with bandwidth of 40 MHz. The bandwidth of this output is matched to the sampling frequency of the CAEN 1724 digitizer sampling at 100 MS/s
- Discriminated low-voltage-differential-signals (LVDS), with a minimum pulse duration of 4 ns. The discrimination threshold is remotely programmable. These signals are sent to the trigger unit and scalars for monitoring

All outputs are tuned to match the -2 to 1 V dynamic range of the digitizers. The typical output noise is approximately 1 mV, 50% of which is due to the digitizer.

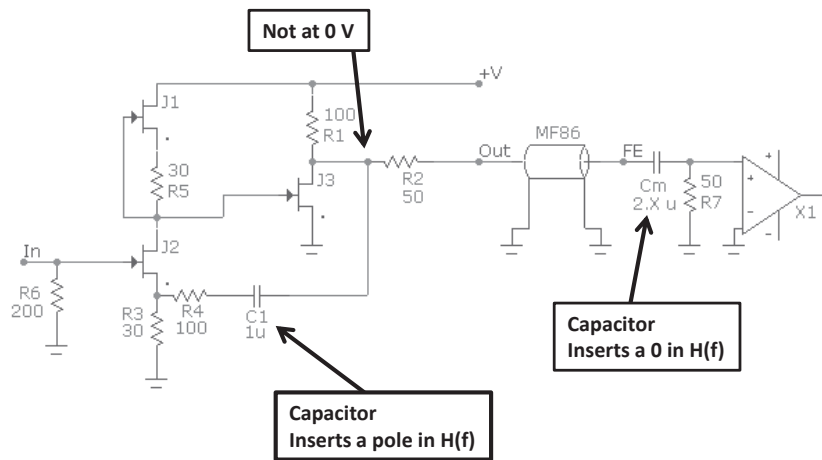


Figure 5. The coupling circuit between the pre-amplifier and the amplifier

3.1.4. Digitization The $\times 10$ gain signals are sent to CAEN V1720 250 MHz 12 bit waveform digitizers [32] and the low gain signals sent to CAEN V1724 100 MHz 14 bit digitizers. Both digitizer types are one unit 6U VME64X VME modules, servicing eight channels. They have circular memory buffers of 10 Ms/ch, and are locally FPGA compliant. The use of two digitizer types extends the dynamic range, providing a linear response between 1 and 10,000 pe, capturing signals without saturation from both LAr and Ar gas. The large dynamic range also improves calibration options and provides a more detailed study of backgrounds.

The multiple ADCs are synchronized with a common 50 MHz clock and external trigger. They run in parallel and require three common control signals: a “Trigger”, a “Run-enable”, and a “Clock”. The Trigger and Run-enable can be either TTL or NIM level signals, however the clock signals are differential LVDS. The distribution of all signals requires equal delays in a star-like topology in order to keep timing synchronization.

4. Veto Systems

As described above, there are two embedded veto systems, a water Cherenkov detector (CTF), and a liquid scintillator detector (LSV). The effectiveness of these veto systems is described in [30] and included references. The CTF is an active veto, tagging penetrating cosmic muons and cosmogenically produced charged showers in materials surrounding DS, and shielding the TPC and LSV from external radioactivity. The CTF is a cylindrical, steel tank, 11 m in diameter and 10 m high, filled with 1000 tons of high-purity water. It is instrumented along the floor and bottom half of the cylindrical wall by 80 ETL-9351 8 inch PMT [31]. Studies revealed little spatial dependence of the PMT placement, so they were spaced more-or-less equally apart. The walls are covered with reflecting Tyvek [33] sheets. The veto electronics for both the LSV and CTF are located in the CoR.

The LSV is a 4 m diameter, stainless steel sphere which lies inside the CTF and encloses the TPC. It is filled with liquid scintillator and instrumented with 110 Hamamatsu R5912-HQE-LRI 8 inch PMT [34]. The interior walls of the sphere are covered with reflecting Lumirror sheets [35].

The LSV is designed to moderate, capture, and thus provide a veto signal for neutrons which might enter, or exit, the TPC. Neutrons can be thermalized by scattering from protons in the scintillator liquid, and are efficiently captured by ^{10}B nuclei. Capture on ^{10}B proceeds to the ^7Li ground state (gs) and a ^7Li excited state with branching ratios of 6.4 % and 93.6 %, respectively. The ground state decays by emitting a 1775 keV α particle, and the excited state decays with emission of a 1471 keV α particle and a 478 keV γ .

The measured LSV light yield is (530 ± 20) pe/MeV. Scintillation light produced by the nuclear emission products of the $^7\text{Li}(\text{gs})$ decay is quenched and collected as an energy equivalent deposition of a β induced ionization. Thus, 30-60 keV energies correspond to 15-30 pe. Neutrons can also capture on hydrogen with the emission of a 2.2 MeV γ -ray yielding approximately 1100 pe.

Most photons are collected in about 100 ns, but the tail of the distribution extends some 300 ns, and must be considered when designing the appropriate dynamic range of the acquisition electronics. For example, the average number of photons per channel in an event with energy < 400 keV is typically less than one, but can increase by more than an order of magnitude when a neutron is captured near a PMT. In addition, a muon crossing the LSV produces a large signal corresponding to approximately 2 MeV per transit-length in the scintillator. Thus the veto electronics must be able to efficiently detect a signal as small as 0.3 pe with a time resolution of better than 0.5 ns, but should gracefully handle signals which saturate the front end electronics. Although the most important events occur at low energy, the system should recover from saturation in less than 2 μ s.

Good timing is also important in order to obtain track reconstruction. This requires knowledge and stability of the relative time differences between PMTs for both vetoes [36]. Therefore time alignment and synchronization among channels must have a precision of ≤ 0.3 ns, and remain stable for at least a 24 hour period.

4.1. Veto Front-end Electronics

Output signals from the veto PMTs are AC coupled directly to amplifiers through approximately 40 m of low dispersion, 50 Ω , coaxial cable [37]. The front end analogue boards (FEAB) and front end digital boards (FEDB) are designed to match the input timing, noise, and impedance of the PMT signals, but more importantly they match the bandwidth of the waveform digitizers. One PCB (board) contains 16 channels arranged in 2 rows of 8 channels, and has 8 layers with dimensions 274 \times 274 mm. Figure 6 is a schematic diagram of signal flow from the PMT through the FEAB to the FEDB.

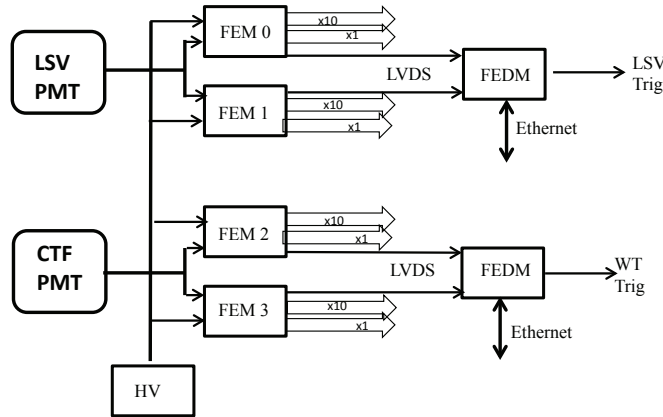


Figure 6. A block diagram of the Veto electronics system

The FEAB configuration uses 3 Texas Instruments operational amplifiers per channel [38], one with a gain of 1 and two with a gain of 10. The x10 signals are split [39] providing digitizer inputs, monitors, discriminated outputs, and a summed signal for 16-channels. The circuit has 230 MHz bandwidth and a total noise of 200 μV_{rms} . A linear power

supply, able to deliver 15 A with a dual voltage ± 7.5 V, was constructed to mitigate the signal noise. Discrimination uses a dual, voltage comparator [40] with differential output. The signals are sent by LVDS to the digital board. The discrimination threshold is set using a standard I²C bus with an 8 bit DAC. The rear panel of the FEAB has 16 HV connectors which connect the PMT cables directly to the CAEN A1536 High Voltage Boards [41] which are housed in a CAEN mainframe [42].

4.1.1. Veto Digital Boards The FEABs are controlled by a FEDB. These boards contain a Xilinx Spartan 6 FPGA [43] which is used to generate a veto trigger using logical patterns from the discriminator inputs from the FEAB. Input signals arrive at a mezzanine board on the FEDB where they are duplicated, one sent to a time to digital converter (TDC) and the other converted to the single-ended TTL standard of the FPGA. A master clock signal is used for global timing. The FPGA is interfaced to a PIC-32 micro-controller (μ C) [44] via an I/O bus controlled by the μ C. Both the FPGA and μ C firmware were developed for the project.

Some slow control operations are also handled by the FEDB, and these are managed by the μ C using Ethernet and FPGA connections. The μ C runs a single process which obtains an IP address from the LAN DHCP and acts as a command interpreter, waiting for incoming socket connections on a specific port. In addition to resolving commands, the μ C dialogues via I²C to set and read the 12 bit channel input offset-compensations and the 8 bit discriminator thresholds. It also controls an alphanumeric display via an I²C bus to display data and status of a specific channel.

4.1.2. Digitization The PMT signals from both the CTF and LSV are amplified by the FEAB boards and their waveforms digitized by commercial National Instruments PXIe-5162 modules [45]. The x10 channels are placed in 4 PXIe chassis, with two chassis used for the CTF and two for the LSV. Each chassis houses analog inputs for the waveform digitizers (56 for the LSV, 40 for the CTF) and connects to digital TTL lines for the trigger and synchronization interface. The waveform is sampled at 1.25 GS/s (800 ps/sample) with 10 bit resolution (2 byte). Each waveform digitizer has 4 BNC input channels and is sampled asynchronously and continuously. When a trigger is received, a block of samples within an acquisition window is stored in the digitizer memory buffer. The timing of the trigger with respect to this window is configurable, so that samples prior to a trigger can be stored. The input voltage range for each channel can be selected as either 0.1, 0.2, 0.5, 1, 2 or 5 V peak to peak, with the usual amplitude set between 0.1 and 0.9 Volt. [44]

4.1.3. Zero Suppression A zero suppression algorithm is applied to reduce the quantity of stored data. This operation has a user specified threshold, minimum width, and number of collected pre and post-samples. When the waveform crosses, and stays above a threshold for a specified number of samples (minimum width), the algorithm returns the entire waveform between the upward and downward threshold crossings including a specified number of pre and post-samples. If the waveform goes below and then back above threshold before the specified number of post-samples are collected, the algorithm waits for the waveform to drop back below threshold again before counting post-samples. Therefore, if two pulses

appear on the same channel with overlapping zero suppression windows, they are combined into one larger pulse. All the samples outside the accepted sample pulse widths are discarded. Data are usually taken with a zero suppression threshold of -30 or -50 mV, a minimum width of 4 samples (3.2 ns), and with pre and post-sample widths set to 25 ns.

4.1.4. Veto Controller The NI PXIe-8133 controller [46] is an Intel Core i7-820QM quad-core processor (1.73 GHz frequency), with 3.06 GHz (single-core turbo-boost) running the Windows7 OS. It is housed in a NI PXIe-1075 chassis and connects to the PXIe modules using the PXI Express system. Two gigabit Ethernet ports are used to connect the controller to the local area network. The data acquisition code in the controller, asynchronously collects data from the digitizers and performs zero suppression. The zero suppressed waveforms are then transmitted in a packet to the veto builder via TCP/IP. The controller also receives commands from a master run controller.

Each processor controls up to 14 digitizer boards, one NI PXIe-6674T timing and synchronization module [52], and one NI PXIe-7961R FlexRIO FPGA module [48]. The veto system requires four PXIe chassis for the 190 channels, with each chassis housing one PXIe controller.

5. Trigger

The TPC and veto systems can operate independently, but must be synchronized in order to correlate TPC events with veto signals. Although the two systems are physically displaced, the main difference between the systems is the width of the data acquisition window, which for a TPC event is $\geq 350 \mu\text{s}$ while the veto has either a “short window” of $6.5 \mu\text{s}$ or a “long window” of $70 \mu\text{s}$. The FlexRIO FPGA PXIe-7961R module is similar to the CAEN V1495 module, as both allow trigger logic to be programmed into an on-board FPGA. TPC triggering is obtained by logically processing signals received from the front-end, to determine the number of hits within a set timing window, and the veto trigger is generated by the FEDB in a similar way. Synchronization between the systems is obtained through a high precision time-stamp obtained from a common 50 MHz clock slaved to a 1 pulse per second (1PPS) signal received from the LNGS GPS. The TPC trigger is always the trigger-master when collecting synchronized data. However, each system can be locally triggered for calibration and testing.

5.1. TPC Trigger

The TPC data acquisition system (DAQ) includes one VME crate containing 5 CAEN V1720, 5 CAEN V1724 modules, a CAEN V1495 [50] logic module, and a V976 NIM-to-TTL fanout. When an analog signal in any of the 38 PMT channels of the TPC crosses a threshold, a logic pulse of fixed width is generated and sent to the CAEN V1495 logic module, which is the trigger master. The TPC trigger in the V1495 is obtained by firmware processing any selected set of these digitized PMT “hits” by compiling a running count of these hits within a sliding window. When the running count crosses a defined threshold, a trigger pulse is initiated and a latch generated to inhibit further triggers until the active trigger is processed. The parameters used in the FPGA trigger firmware are listed in Table

1. Parameters marked with [+] can be modified by inputs through the VME interface to the V1495. The TPC V1495 trigger module is the trigger master for both TPC and Veto systems. It includes appropriate dead time in the data acquisition window for either LSV or CTF Veto trigger types in order to prevent trigger overlap.

Table 1. Parameters used in the TPC Logic unit to determine a trigger. Items marked with a [+] can be modified by the VME interface to the logic unit

Parameter	Value
Number of Channels (2 spares)	40
Input Signal	LVDS
Minimal Input Pulse Width	5 ns
Channel Mask Register [+]	40 bit
Time Window (min, max, step) [+]	10, 150, 10 ns
Majority Trigger (low threshold) [+]	1 to 39 channels
Majority Trigger (High Threshold) [+]	1 to 39 channels
Trigger Bit Pattern	40 bit

The master V1495 trigger module increments a trigger-number (Trigger-ID) for each processed trigger. This Trigger-ID is sent to the veto system so that all veto events within the TPC acquisition window are marked with the same ID. The lower eight bits of the trigger number are sent to the V1720 as an 8-bit TPC trigger ordinal to further correlate an ADC event with the trigger. There are also different Trigger-type identifiers as described in the next sections.

6. G2 Trigger

The G2 trigger provides a method to study signals and backgrounds within a selected energy range. As an example, it can tag events with high-multiplicity S2 signals. The G2 trigger is based on summing hits from all enabled TPC discriminator channels occurring within a fixed time window. The window is opened after a pre-trigger is generated by a TPC majority trigger. The trigger logic uses the same discriminator signals which formed the TPC Majority trigger logic. A block-diagram of the G2 trigger logic is shown in Figure 7. The trigger logic follows the following steps.

- The trigger pattern is latched in an internal register after a positive TPC majority logic condition generates a pre-trigger.
- A time window of 1 to 5 μs is immediately generated by a gate generator and used to inhibit other TPC pre-triggers.
- 7-bit counters (one for each of the 38 channels plus 2 spares) start counting hits within the window. The counters either stop at the end of the window, or stop when a counter reaches a maximum value of 127.
- After the window closes, a sequencer scans the counters, summing their values. The TPC pre-triggers remain inhibited by an adder busy signal for another approximate 0.85 μs .

- The resulting sequencer sum is compared to two thresholds. If the sum exceeds a high threshold a “High” multiplicity G2 pre-trigger is generated. If the sum is less than the high threshold, but exceeds the low threshold a “Medium” multiplicity G2 pre-trigger is generated. If the sum is lesser than the Low threshold, a “Low” multiplicity G2 pre-trigger is generated.
- Both the High and Medium trigger types can be pre-scaled by separate, programmable factors. The triggers are then provided to the system trigger logic and used in the trigger selection.
- The process re-starts after the pre-scale window closes and the counters are initialized.

The dead time associated with any G2 trigger is equal to the sum of the time window, the 0.85μ adder busy, and the G2 acquisition window inhibit. The G2 acquisition-window-inhibit setting is equal to the V1720 ADC acquisition window setting.

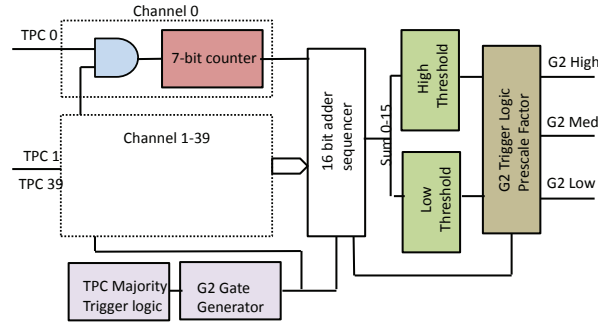


Figure 7. A block diagram of the G2 trigger logic

6.1. Veto Trigger

Hardware veto trigger signals from the FEDB of the LSV and CTF are combined by the veto V1495 and sent to the TPC master V1495 located in the CLR. When a Veto trigger is received, all inputs to the V1495 are evaluated and if appropriate, a separate trigger signal, using Trigger-type bits, is stored in the Trigger-ID. Then a trigger signal and Trigger-ID are sent back to the Veto V1495 Module in the CoR. These are passed to another veto V1495 in the CoR which is used to create copies of the signals and deliver them to each of the 4 PXIe timing modules in the 4 NI PXIe crates. Finally they are distributed to all the PXIe modules in the crates through an internal bus. The PXIe timing modules in the crates also receive the 50 MHz clock, and the 1PPS signal. The veto trigger has the 2 operational modes given below.

- TPC-only-mode.** In this configuration the trigger rate is determined by the internal activity of the TPC. The length of the data acquisition window is set to $45 - 70 \mu s$ to detect prompt and delayed events in the veto which are correlated to TPC activity;
- Pass-through-mode** In this configuration, the LSV and CTF triggers are logically combined (ored) and used as the input trigger to the master V1495. For this mode, the input trigger is determined by the LSV trigger rate. The length of the data

acquisition window is set to $4.5 \mu\text{s}$ in order to acquire the entire scintillation signal and must be adjusted to account for the delay in the hardware trigger.

The veto FPGA has internal FIFO memory used to store the Trigger-ID for each incoming Veto trigger. This memory is read for each event to provide a trigger marker. The veto V1495 decodes the Trigger-ID and places it in the memory for readout via the VME bus for inclusion in the TPC data stream. A 1PPS signal from the LNGS GPS receiver is used to synchronize the V1495 and the veto FPGA modules.

6.2. Synchronization

Figure 8 shows the generation and flow of trigger signals. Unless otherwise noted, signals in the block diagram are active high TTL, ECL or LVDS. There are four FPGA-based trigger logic units. These are;

- (i) TPC V1495 trigger module located at the TPC site (CLR);
- (ii) V1495 trigger module located at the Veto site (CoR);
- (iii) Veto Fanout V1495 module located at the veto site (CoR);
- (iv) Veto FPGA PXie-7961 logic module located in the PXIe crate (CoR)

A 32-bit Trigger-ID is generated for each trigger, acquired by the PXIe timing module, and routed to the veto FPGA for decoding. The time stamps and the Trigger-ID are saved in a DMA buffer in the veto FPGA and are read asynchronously by Veto DAQ. Thus, the Trigger-ID is read out via the VME bus as a part of the TPC data stream, and the same Trigger-ID and the trigger signal are also available for the Veto DAQ readout via a digital adapter module, NI 6583 [51], attached to a veto FPGA. A 24-bit “Event-counter” is programmed to count all incoming triggers for each event. This allows the same event to be correlated between different ADCs as they all have identical time tags and event counters which are stored in the data header. Both of these counters are synchronized at the beginning of the run by the external Run-enable signal, and all systems are kept in synchronization using a “star” distribution with equal time delays of Clock, Trigger and Run-enable signals. The TPC V1495 trigger output is enabled at the same time as the Run-enable signal and the veto system receives Run-enable signal from the TPC V1495 trigger.

It is necessary to inhibit triggers when any ADC memory is full. This is accomplished using a chained “or” of the ADC memory full signals and firmware in the V1720 TPC ADCs. Without these signals it would not be possible to guarantee event synchronization between two sub-systems. Generation of any trigger type is inhibited for an appropriate time after a trigger is issued.

Three counters are recorded and used to create a time stamp for each trigger. These are listed below.

- The 1PPS counter counts the number of seconds elapsed between the trigger and Run-enable signal. The Run-enable signal occurs at run-start so this counter represents the number of seconds between the start of the run and the trigger.
- The GPS fine-time counter counts the number of 50 MHz clock cycles elapsed between the trigger and either the Run-enable or 1PPS signal. This selection is determined by

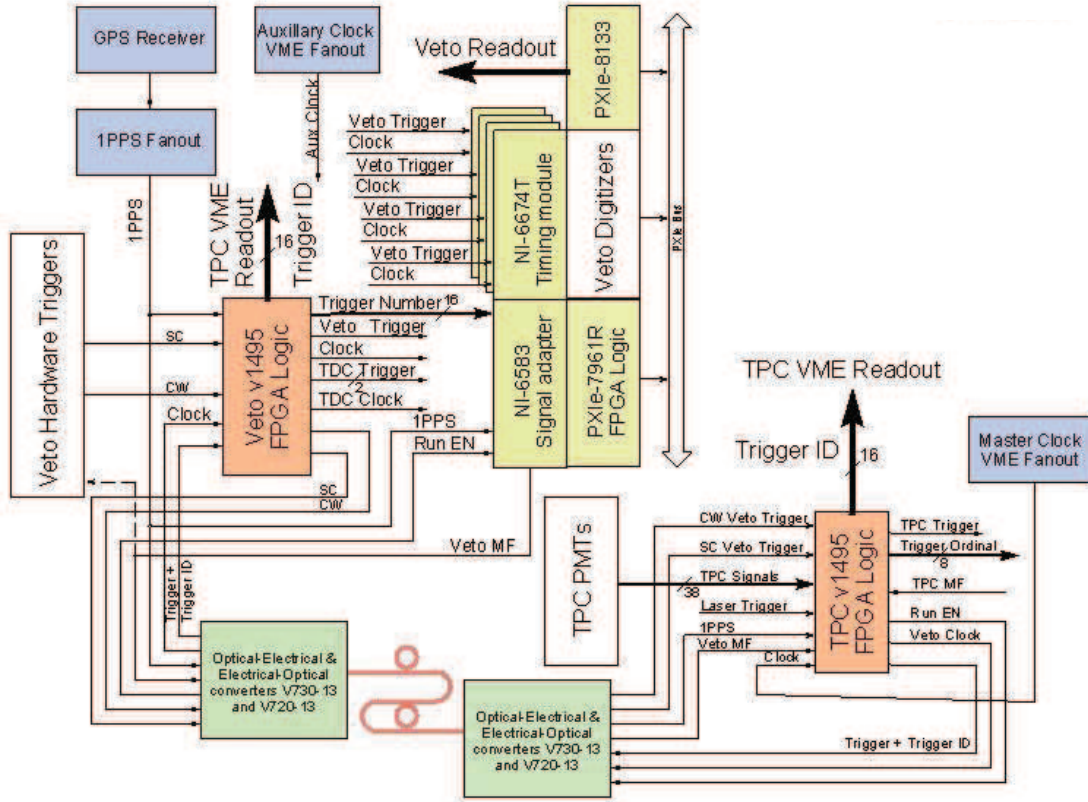


Figure 8. A block diagram showing the trigger connections scintillation vetoes and the TPC cryostat

whichever signal occurs last. The fine-time counter represents the number of 20ns bins between either the Run-enable or 1PPS signal depending on the selected signal.

- The GPS one-second-counter counts the number of 50 MHz clock cycles between the 1PPS signal occurring just prior to the Run-enable signal and the Run-enable signal itself. This counter is used to provide the number of 50MHz cycles between a prior 1PPS signal and the following Run-enable signal.

The counters are stored in the veto FPGA memory, and provide the time of a trigger with respect to the run-start with a precision of 20 ns. This creates a unique time-stamp for a triggered event. Identical time stamps are computed by TPC and veto DAQ systems, so that synchronization of events can be maintained.

6.3. TDC

A secondary data stream for the Veto system is implemented using TDCs. One of the discriminated FEDB veto outputs from each channel is connected to a CAEN V1190 multi-hit 128 channel TDC [53]. The two 1190 modules are located in the CoR and connect to

the TPC V1495 trigger unit through the local V1495 fanout logic unit. This secondary system does not replace the main veto readout but provides a back-up system and solves some TPC integration issues. The system provides an independent data stream for the LSV and CTF Vetoes, and is synchronized to the TPC trigger providing a check on the efficiency of the main veto trigger. Thus a TPC event has direct mapping to the TDC data, and is correlated to the veto ADC stream, solving a problem when the veto triggers before a TPC trigger is generated.

6.4. Clock

The clock and fan-out, CFM [55], is an “in-house”, single width 6U VME module. The input accepts TTL, LVTTTL, or CMOS signals with selective 50 or 10K Ω termination. In addition a second connector accepts standard LVDS signal and is pin compatible with the CAEN V1720 ADC pinouts. The CFM uses a Texas Instruments CDCE906 programmable 3-PLL clock synthesizer/multiplier/divider [54] and is a source of the output signals. The CDCE906 operates in various modes including “PLL-bypass” and “Divider”. Jumper pins allows the input frequency from either from an external source or from an on-board 100 MHz OCXO AOCJY2 [56] quartz crystal oscillator. The block-diagram of the CFM design is shown in Figure 9. A 2x8-channel CAEN V976 fanout module is used to distribute Trigger and Run-enable signals.

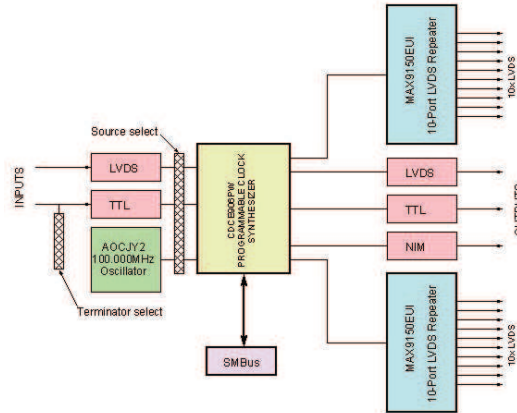


Figure 9. The block diagram of the CFM module

7. Data Acquisition

It is assumed that the TPC and veto systems run independently at selected times, collecting data with their own triggers. For this reason, two modes of operation are available, which can be selected using a run mode register stored at each site.

- (i) The system can run in local mode, in which each sub-system receives and records only its own triggers; or

- (ii) The system can run with event synchronization with the TPC DAQ system as the master.

7.1. TPC DAQ

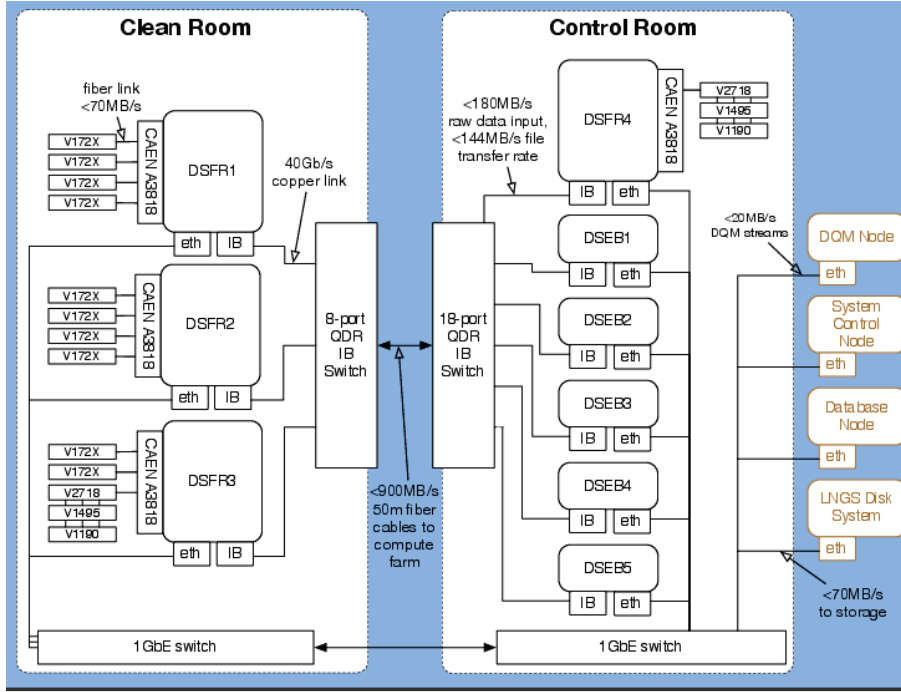


Figure 10. A Block diagram of the DAQ illustrating the data flows between the CLR, CoR, Control, and Storage

The DAQ is designed for high parallelization, as illustrated in Figure 10. There are five 8 channel CAEN V1724 digitizers and five 8 channel V1724 digitizers which are read via optical cable into the PCI interface [57] of three local computers. One of these CLR computers is also optically connected to the VME bus through the CAEN 2718 crate controller, sharing information with the V1495 logic trigger module and therefore with the CAEN 1190 multi-hit TDCs in the CoR. Digitizer output signals are sent to fragment servers and are multiplex through a 40 Gb optical fiber from the CLR to the CoR. All computers run the ArtDaq software [58] tools which are used to transfer data from the front-end computers through the DAQ system to disk, and provide a selection of events for online data quality monitoring, Figure 11. The event builder compresses the data and an “aggregator-server” puts the events in sequential order storing them on disk. The aggregator also provides events for online monitoring, including run parameters from disk files, and closes files at appropriate times during a run.

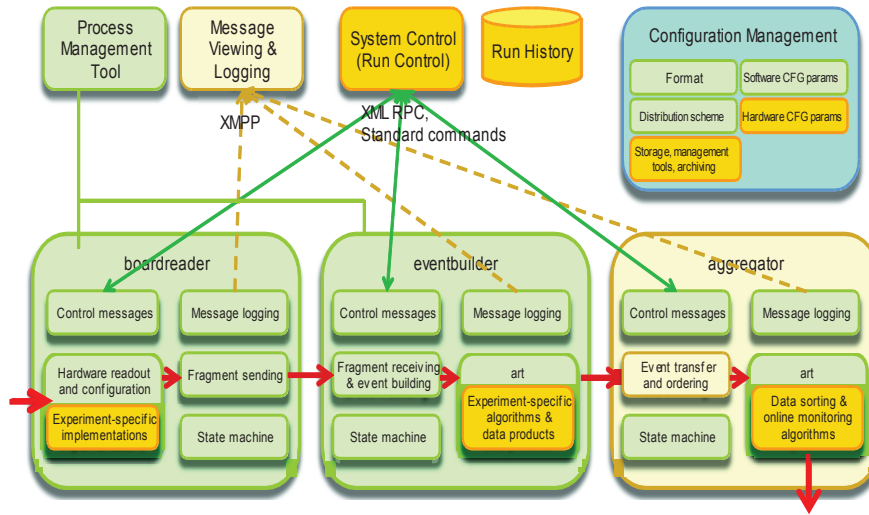


Figure 11. A Block Diagram of ArtDaq operations

7.2. Veto DAQ

The veto DAQ architecture is designed to acquire data from 4 different PXIe controllers, preserving synchronization between each device and the TPC. The system software is constructed of two software elements: acquisition-and-readout software and builder software. Software is developed in LabVIEW, and conforms to LabVIEW coding and documentation standards. The Veto DAQ uses the parallelism inherent in LabVIEW to perform the main operations.

The readout software has the following tasks:

- it acts as a server to listen for commands from the run controller (e.g. request to start and stop data taking, communicate the status of the system, or provide the number of acquired events);
- it checks CPU, and memory usage in the controller;
- it drives a state machine to perform the data acquisition operations (e.g. initialize hardware, fetch data, stop, etc.);
- it communicates with the FPGA module, retrieving the Trigger-ID and the time stamp of the event;
- it performs zero suppression on the acquired data;
- it bundles zero-suppressed data from different digitizers in a data fragment structure, which contains the time-stamps and the Trigger-ID of the event;
- it sends data to the veto builder over the network;

Each veto readout software is installed in the PXIe controllers and is automatically loaded when the controller boots. The veto DAQ architecture is based on a producer-consumer data flow driven by a state machine. Communication over the network uses the LabVIEW Simple Messaging Reference Library (STM). The content of a message is parsed,

evaluated, and a response message broadcast. During data acquisition, data fragments from every chassis are collected by the Veto builder. The builder checks the consistency of the Trigger-ID and timestamps of the data fragments. Finally, the events are entered in sequential order and written on disk in a custom binary format.

8. Run Control

The DAQ sub-systems are handled by a common run controller which is configured to permit differential data acquisition modes.

- (i) Global runs, where the TPC and veto triggers are correlated, and
- (ii) Local runs, where sub-detectors can be run independently.

The run controller handles the initialization, start-up, and stopping of data acquisition, and logs to the experimental data base relevant run parameters, such as the TPC and Veto configuration. The run controller also supervises the data acquisition. When a sub-systems displays unusual behavior, data acquisition is stopped and the DAQ sub-systems are reset and re-initialized. The run controller is developed in LabVIEW, and conforms to LabVIEW coding and documentation standards. Communication over network with TPC sub-systems is performed using the XML-RPC protocol, while communication with Veto sub-systems is performed using LabVIEW STM protocol.

9. Summary

This paper reports the electronics and data acquisition systems developed for the DarkSide-50 DM search. The DAQ involves data collection from a 2-phase LAr TPC which is enclosed by liquid scintillator and water Cherenkov vetos. The paper describes the electronics required to obtain digitized PMT waveforms from the various detector systems, the parallel data flow to an event building computers, system synchronization, event-building, and run control. The full system has been operational several months, and can be controlled remotely. Data capture is stable with a maximum accepted data rate of over 50 Hz, and up to 6 TB of compressed data can be written to disk per day. A novel cryogenic pre-amplifier was implemented which provides extremely low noise and signal distortion. A dynamic range of over 2000 is obtained using dual digitizers for each TPC channel.

10. Acknowledgements

This work was supported in part by grants from US National Science Foundation Nos. 1004051, 1242571, 1314268,, 1314501, 1314507, 1314479, 1314752, the US Department of Energy Nos. DE-FG02-91ER40671, DE-AC02CH11359 and the Istituto Nazionale di Fisica Nucleare (Italy.). The collaboration gratefully acknowledges the support of Nicola Cescato, Fabio Cortinovis, Thierry Debelle and Andrea Nobile of National Instruments.

- [1] The Dark Matter Scientific Assessment Group, Report on the Direct Detection and Study of Dark Matter, <http://science.energy.gov/hep/hepap/reports/> (2007).
- [2] M. W. Goodman and E. Witten, Phys. Rev. D 31 (1985) 3059
- [3] Z. Ahmed et al. (CDMS Collaboration), Phys. Rev. D 83 (2011) 112002.
- [4] E. Armengaud et al. (EDELWEISS Collaboration), Phys. Rev. D 86 (2012) 051701(R).
- [5] G. Angloher et al. (CRESST Collaboration), Eur. Phys. J. C 72 (2012) 1971.

- [6] R. Bernabei et al. (DAMA/LIBRA Collaboration), Eur. Phys. J. C 67 (2010) 39 (2010)
- [7] S.C. Kim et al. (KIMS Collaboration), Phys. Rev. Lett. 108 (2012) 18.
- [8] S. Archambault et al. (PICASSO Collaboration), Phys. Lett. B 682 (2009) 185.
- [9] E. Behnke et al. (COUPP Collaboration), Phys. Rev. Lett. 106 (2011) 021303.
- [10] C.E. Aalseth et al. (COGENT Collaboration), Phys. Rev. Lett. 106 (2011) 131301.
- [11] E. Aprile et al., (XENON Collaboration), Phys. Rev. Lett. 107 (2011) 131302.
- [12] G.J. Alner et al. (ZEPLIN Collaboration), Astropart. Phys. 28 (2007) 287.
- [13] D.S. Akerib et al. (LUX Collaboration), arXiv:1210.4569
- [14] www-sk.icrr.u-tokyo.ac.jp/xmass/.
- [15] <https://deapclean.org>.
- [16] A. Rubbia, J. Phys. Conf. Ser. 39 (2006) 129.
- [17] <http://darkside.lngs.infn.it/>; arXiv (2014) 1410.0653v1.
- [18] M.G. Boulay and A. Hime, Astropart. Phys. 25 (2006) 179.
- [19] G. Bellini et al JCAP05 (2012) 015.
- [20] G. Bellini et al JCAP08 (2013) 049.
- [21] D. Akimov et al. (DarkSide Collaboration), Astroparticle Physics Journal 9 (2013) 44.
- [22] J. Xu et al., ArXiv (2012) 1204.6011; H.O. Back et al., ArXiv (2012) 1204.6024.
- [23] G. Alimonti et al. (Borexino Collaboration) Astropart. Phys. 16 (2002) 205 (2002).
- [24] G. Bellini et al. Phys Rev D 89 (2014) 112007 doi:10.1103/PhysRevD.89.112007.
- [25] G. Alimonti et al. (Borexino Collaboration) NIM A 600 (2009) 568593.
- [26] G. Bellini et al. (Borexino Collaboration) JINST 6 (2011) 05005.
- [27] R. Acciam et al. Proceedings of the 2nd International Conference on Technology and Instrumentation in Particle Physics TIPP (2011).
- [28] <http://www.cirlex.com>.
- [29] Multiflex 86 LowLoss <http://www.koax24.de/en/coaxial-cable/overview-50-o/24-32-mm-gr2/multiflex-86.html>
- [30] Anton Empl et al., ArXiv (2014) 1406.6081; JCAP 8 (2014) 64.
- [31] borex.princeton.edu/public-docs/theses/.../pocar_phd_chapter2.pdf.
- [32] http://www.caen.it/Home/Products/Mdular_Pulse_Processing_Electronics.
- [33] http://phy.duke.edu/~schol/superk/alvaro_thesis.pdf.
- [34] <http://http://www.hamamatsu.com/jp/en/product/category/index.html>
- [35] <http://www.toray.jp/films/en/properties/lumirror/>.
- [36] G. Bellini et al. Phys Rev D 89 (2014) 112007; G. Alimonti et al. (Borexino Collaboration) NIM A 600 (2009) 568; G. Bellini et al. (Borexino Collaboration) JINST 6 (2011) 05005
- [37] arXiv (2008) 0806.2400.
- [38] <http://www.ti.com/product/th3201>, ths3202.
- [39] <http://www.datasheetarchive.com/LMH6559-datasheet.html>.
- [40] http://www.analog.com/static/imported-files/data_sheets/ADCM567.pdf.
- [41] <http://www.caen.it/Home/Products/>.
- [42] <http://www.caen.it/Home/Products/>.
- [43] http://www.xilinx.com/Products/Programmable_Devices/FPGA.
- [44] ww1.microchip.com/downloads/en/DeviceDoc/30009904p.pdf.
- [45] <http://www.ni.com/pdf/manuals/373858a.pdf>.
- [46] <http://www.ni.com/pdf/manuals/372870b.pdf>.
- [47] <http://www.ni.com/pdf/manuals/373089b.pdf>.
- [48] <http://sine.ni.com/nips/cds/view/p/lang/en/nid/208165>.
- [49] <http://www.ni.com/pdf/manuals/372537b.pdf>.
- [50] <http://www.caen.it/csite/CaenProd.jsp?idmod=484&parent=11>.
- [51] <http://www.ni.com/pdf/manuals/375506c.pdf>.
- [52] <http://www.ni.com/pdf/manuals/373089b.pdf>.
- [53] <http://www.caen.it/csite/CaenProd.jsp?idmod=787&parent=11>.
- [54] <http://www.ni.com/pdf/manuals/323452a>.
- [55] B. Baldin, "Clock Fanout Module", Private Communication, November 2012.
- [56] <http://www.microcrystal.com/index.php/en/products/oscillators/ocxo>.
- [57] <http://www.caen.it/csite/CaenProd.jsp?idmod=627&parent=51>.
- [58] K. Biery, et al., Real Time Conference (RT), 2012 18th IEEE-NPSS.